JGR Space Physics

RESEARCH ARTICLE
10.1029/2021JA029351

The Signal of Solar Storms Embedded in Cosmogenic Radionuclides: Detectability and Uncertainties

F. Mekhaldi[1], F. Adolphi[2], K. Herbst[3], and R. Muscheler[1]

[1]Department of Geology-Quaternary Sciences, Lund University, Lund, Sweden, [2]Helmholtz Centre for Polar and Marine Research, Alfred Wegener Institute, Bremerhaven, Germany, [3]Institut für Experimental und Angewandte Physik, Christian-Albrechts-Universität zu Kiel, Kiel, Germany

Key Points:

- We model the production rate of the radionuclides ^{10}Be, ^{14}C, and, ^{36}Cl by 59 ground level enhancement events
- We provide a sensitivity test for ice-core ^{10}Be and ^{36}Cl produced by extreme solar storms and infer detection limits
- ^{36}Cl is best to detect past solar storms and its lack of data may lead to an underestimate of the occurrence rate of softer events

Supporting Information:

Supporting Information may be found in the online version of this article.

Correspondence to:

F. Mekhaldi,
florian.mekhaldi@geol.lu.se

Citation:

Mekhaldi, F., Adolphi, F., Herbst, K., & Muscheler, R. (2021). The signal of solar storms embedded in cosmogenic radionuclides: Detectability and uncertainties. *Journal of Geophysical Research: Space Physics*, *126*, e2021JA029351. https://doi.org/10.1029/2021JA029351

Received 26 MAR 2021
Accepted 6 JUL 2021

Abstract The threat that solar storms pose to our ever-modernizing society has gathered significant interest in the recent past. This is partly due to the discoveries of large peaks in the content of cosmogenic radionuclides such as radiocarbon (^{14}C) in tree rings and beryllium-10 (^{10}Be) and chlorine-36 (^{36}Cl) in ice cores that were linked to extreme solar storms dated to the past millennia. To better assess the threat that they represent, we need to better quantify the relationship between their energy spectrum and their magnitude with respect to the content of the radionuclides that we measure in environmental archives such as ice cores. Here, we model the global production rate that the 59 largest particle storms coming from the Sun have induced for ^{10}Be, ^{14}C, and ^{36}Cl during the past 70 years. We also consider the deposition flux in ^{10}Be and ^{36}Cl over the high latitudes where all Greenland ice cores are located. Our analysis shows that it is unlikely that any recent solar particle event can be detected in ^{10}Be from ice cores. By relating these values to empirical data from ice cores, we are able to quantify different detection limits and uncertainties for ^{10}Be and ^{36}Cl. Due to different sensitivities to solar energetic particles, we assess that ^{10}Be may only be suitable to detect a limited number of extreme solar storms, while ^{36}Cl is suitable to detect any extreme particle event. This implies that the occurrence-rate estimates of extreme solar storms, based mainly on ^{14}C and ^{10}Be, relate to a small population of potential events.

Plain Language Summary Solar storms occur when the sun expels charged energetic particles and magnetic material towards Earth. They are a threat to astronauts, spacecraft, and electronic infrastructures on the ground. On rare occasions, solar storms can lead to a significant atmospheric production of radioactive isotopes. If extreme enough, this signal can be retrieved from environmental archives such as ice cores and tree rings. The last known instance of this occurred about a millennium ago. It is therefore paramount to better understand to what extent solar particles can produce these isotopes so that we can, in turn, better identify and quantify the events that generated them. In this study, we combine energy distribution profiles of 59 contemporary solar storms with production functions of the previously mentioned isotopes to model their atmospheric production. This enables us to assess the minimum magnitude of a solar storm required to be detected in ice cores. We also show that one of these isotopes-chlorine-36 can be used to detect a considerably wider range of extreme events, relative to the other isotopes. These results have important implications for our current assumptions on the likelihood of an extreme solar storm to hit Earth in the near future.

1. Introduction

Although the Sun is considered a relatively quiescent star, it can produce electromagnetic and particle storms that are large enough to wear down and even damage our technological infrastructure significantly. For instance, shocks driven by coronal mass ejections (CME) can accelerate solar energetic particles (SEP) that reduce the lifetime of space-borne instruments (Reames, 2004). These SEPs can also be accelerated by intense solar flares. In the case of CMEs, the structure of their plasma and magnetic field environments can lead to severe geomagnetic storms that pose an additional challenge to our electronic infrastructures on the ground (e.g., Shea & Smart, 2012). The CME of March 1989, for example, caused a 9-h blackout in the province of Québec in Canada, while the sequence of CMEs in October 2003, commonly referred to as the Halloween storms, have led to a blackout in the city of Malmö (Sweden). In the latter case, the SEPs associated with the events have led to a peak in the counting rates of many ground-based stations of the worldwide neutron monitor network. Such events are known as ground-level enhancement (GLE) events, of which

72 have been listed to date (e.g., http://www.nmdb.eu/nest/gle_list.php; http://gle.oulu.fi), the largest one being the event on February 23, 1956 (GLE no. 05, Meyer et al., 1956; Usoskin et al., 2020).

To document the occurrence of extreme GLEs prior to the use of ionization chambers and neutron monitors in the 1940–50s (Simpson, 2000), we can rely on cosmogenic radionuclides such as ^{10}Be, ^{14}C, and ^{36}Cl. Oftentimes, cosmogenic radionuclides are used to reconstruct the long-term changes in solar activity and in the dipole moment of the geomagnetic field (e.g., Bard et al., 1997; Muscheler et al., 2005, 2016; Steinhilber et al., 2012; Vonmoos et al., 2006). The hypothesis that radionuclides may be produced as a by-product of SEPs reaching the atmosphere was first formulated by Simpson (1960). A few decades later, continuous and quasi-annual measurements of ^{10}Be concentration from the Greenland ice cores Dye3 (Beer et al., 1990, 1998), and NGRIP (Berggren et al., 2009) allowed for the tentative identification of the signal of extreme GLEs from the past (McCracken et al., 2001; Usoskin & Kovaltsov, 2012), though no such robust estimate was possible due to the noise inherent to ice core data (Pedro et al., 2009). More recently, three conspicuous increases in Δ^{14}C (^{14}C/^{12}C corrected for fractionation and decay relative to a standard and noted as Δ in Stuiver & Polach, 1977) have been discovered and dated to 993/4 CE (Miyake et al., 2013), 774/5 CE (Miyake et al., 2012) and 660 BCE (Park et al., 2017). Upon discovery, the three extreme events have been confirmed in various ice cores as peaks in ^{10}Be and ^{36}Cl concentrations (Mekhaldi et al., 2015; Miyake et al., 2015; O'Hare et al., 2019). These ice core data allowed us to confirm that these events were caused by extreme SEP events with a hard spectrum, i.e., a small drop-off in the flux of high energy protons relative to low energy protons. In fact, it has been estimated that these events were at least one order of magnitude stronger than GLE no. 05 (Mekhaldi et al., 2015; Usoskin et al., 2013), with the 774/5 CE peak representing the largest benchmark event at present. At the same time, these events were used to test and, thereafter, reject the hypothesis that nitrates in ice cores can be used as a reliable proxy for SEP events (Mekhaldi et al., 2017), leaving radionuclides as the only robust alternative. Usoskin et al. (2006), Webber et al. (2007), and Herbst et al. (2015) have assessed the contribution of some of the largest GLEs in the global production rate of ^{14}C and ^{10}Be (Herbst et al., 2015; Usoskin et al., 2006), and ^{10}Be and ^{36}Cl (Herbst et al., 2015; Webber et al., 2007). The results from Webber et al. (2007) and Herbst et al. (2015) highlight that the production of ^{36}Cl by SEPs is relatively more enhanced than that of ^{10}Be, because of its higher production-rate sensitivity to incident protons with energies below 500 MeV. This has been confirmed empirically for the three historical events mentioned previously (Mekhaldi et al., 2015; O'Hare et al., 2019). Being mindful that these events all were discovered first with Δ^{14}C measurements from tree rings, the production sensitivity to SEPs of which is close to ^{10}Be (Poluianov et al., 2016) and possibly even lesser (Herbst et al., 2015), we can formulate the hypothesis that additional extreme events with a softer spectrum (i.e., a large drop-off in the flux of high energy protons relative to low energy protons) may be identified in ^{36}Cl from ice cores but not in ^{10}Be or ^{14}C.

Recently, Poluianov et al. (2016) have provided new and consistent yield functions of five cosmogenic radionuclides including ^{10}Be, ^{14}C and ^{36}Cl as a function of atmospheric depth and for energies that span the realm of SEPs and GCRs. In addition, Raukunen et al. (2018) have published spectral parameters for 59 of the currently listed 72 GLEs to fit their integral fluence spectra in rigidity (the momentum of a particle relative to a magnetic field it encounters) using the Band function (Band et al., 1993). Taken together, this allows us to systematically model the expected production signal in ^{10}Be, ^{14}C, and ^{36}Cl for each of these GLEs assuming isotropic irradiation of Earth by SEPs. First, we calculate and compare the global annual production rate in ^{10}Be, ^{14}C, and ^{36}Cl throughout the Space Age, including these GLEs. This first step serves as an update from Webber et al. (2007) that investigated fewer GLEs and used different production functions and fluence spectra. In fact, their global production rate by galactic cosmic rays (GCRs) estimated for ^{10}Be and ^{36}Cl are significantly (around 50%) lower than the recent work presented in Poluianov et al. (2016). This has direct implications in terms of detectability of the SEP signal, which depends on the production rate increase relative to the background, that is the GCR-induced production. Then, we compare the GLE-related production of the Space Age to the signal of the 774/5 CE in ice cores, update the fluence estimates, and infer their uncertainties. Finally, we quantify the difference in detectability of the SEP signal in ^{10}Be and ^{36}Cl data from ice cores and discuss its implication vis-à-vis the assessment of the occurrence rate of extreme SEP events, regardless of spectral dependencies.

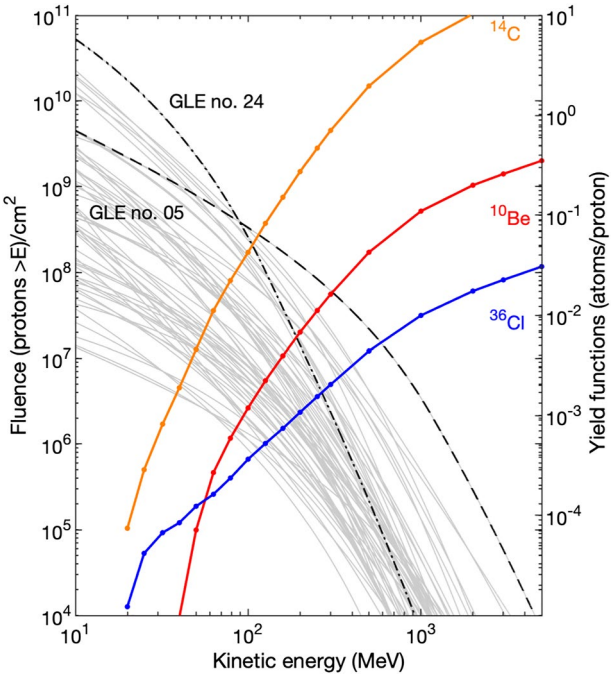

Figure 1. The yield functions of ^{10}Be, ^{14}C and ^{36}Cl from Poluianov et al. (2016) (right *y*-axis) and the integral fluence spectra for the 59 GLEs analyzed in Raukunen et al. (2018) (left *y*-axis). GLE no. 05 is plotted as a dashed black curve while GLE no. 24 is plotted as a dashed-and-dotted black curve.

2. Production Functions

2.1. Production Functions

In this study, we quantify the atmospheric production of the cosmogenic radionuclides ^{10}Be, ^{14}C, and ^{36}Cl by solar energetic particles (SEPs), of varying energy distributions. To achieve this, knowledge of the specific yield function $Y(E_p)$, i.e., the number of produced atoms per incoming particle with energy E_p, as well as of the differential proton flux $J(E_p)$ of several SEP events is required to obtain the differential production $R(E_p)$ (see e.g., Beer et al., 2012; Poluianov et al., 2016; Webber et al., 2007):

$$R(E_P) = Y(E_P) \cdot J(E_P). \quad (1)$$

Recently, Poluianov et al. (2016) provided detailed production functions for different atmospheric depths and various radionuclides including ^{10}Be, ^{14}C, and ^{36}Cl. The atmospheric depth integral of these functions multiplied by π gives us their yield functions (Poluianov et al., 2016) per energetic proton with a given energy, shown in Figure 1. In other terms, these functions predict how many atoms of each radionuclide will be produced by one incoming proton of a given kinetic energy, in units of atoms per primary protons. A comparison in Poluianov et al. (2016) of their yield functions to an earlier study (Webber et al., 2007) shows an overall good agreement for the production of ^{10}Be and ^{36}Cl by SEPs. From Figure 1, it can be seen that the relative production increase of ^{10}Be, ^{14}C and ^{36}Cl with increasing energy beyond 1 GeV is similar. Because most radionuclides produced in the atmosphere result from GCR with higher energies, the relative changes in the production rate due to varying solar modulation and geomagnetic shielding of GCRs are expected to be virtually identical (Masarik & Beer, 1999; Poluianov et al., 2016; Webber et al., 2007). On the other hand, the proton energy dependency of the production of ^{10}Be, ^{14}C, and ^{36}Cl shows disparate patterns for protons <500 MeV that dominate the fluence spectra of SEP events (Figure 1), with ^{36}Cl being relatively more sensitive to incident protons than ^{10}Be and ^{14}C below that energy. This is the effect of a resonance for the production of ^{36}Cl from the target nuclei ^{40}Ar in interaction with protons at ~25 MeV (Webber et al., 2007). We note that the excess in ^{36}Cl production at ~25 MeV, relative to ^{10}Be and shown in Webber et al. (2007), is also present in the recent work of Poluianov et al. (2016). Due to this resonance effect, the expected isotopic footprint of a solar proton event in ice core data is a larger enhancement in ^{36}Cl than in ^{10}Be, relative to the GCR production baseline. Empirical confirmation of this effect stems from the comparison of ^{10}Be and ^{36}Cl concentration data from ice cores for the three extreme "paleo"-events confirmed to date (Mekhaldi et al., 2015; Sigl et al., 2015; O'Hare et al., 2019). In each case, the increase in ^{36}Cl was nearly twofold that of ^{10}Be.

2.2. Fluence Spectra of GLEs

Owing to the publication of a catalog of spectral parameters for most of the observed GLEs (Raukunen et al., 2018), it is now possible to calculate the production of various radionuclides caused by 59 of the 72 GLEs that have been recorded to date. This allows us to investigate the implication of the wide variety of energy distributions, or spectral hardness, of these different events on the atmospheric production rate of radionuclides as well as on their signal expected in ice cores (for ^{10}Be and ^{36}Cl). The omnidirectional event-integrated integral fluence spectra for these 59 GLEs given in Raukunen et al. (2018) are also plotted in Figure 1. As can be seen, GLE no. 05 (date: 1956-02-23) and GLE no. 24 (date: 1972-04-08) are characterized by the highest fluence for protons greater than, and lesser than ~100 MeV, respectively. The spectral hardness of the different GLEs can be described by the spectral index ($SI_{30/200}$) as used previously (Asvestari et al., 2016; Cliver et al., 2020) with F_{30} and F_{200} representing the fluence of protons with energies above 30 and 200 MeV:

$$SI_{30/200} = \log\left(\frac{F_{30}}{F_{200}}\right). \quad (2)$$

A list of $SI_{30/200}$ for the 59 GLEs listed in Raukunen et al. (2018) is available in Cliver et al. (2020). A reassessment of the fluence spectrum of GLE no. 05 was published recently (Usoskin et al., 2020) that differs from the fluence spectrum presented in Figure 1. This is especially true for proton rigidities above 1 GV that are rare and hence, not dominant for the atmospheric production of radionuclides by solar energetic protons.

To calculate the production of ^{10}Be, ^{14}C, and ^{36}Cl by each of these GLEs, we differentiate the integral fluence spectra in units of protons/cm^2 shown in Figure 1 to fluxes in units of protons/cm^2/MeV/sr/s. Following Equation 7 from Poluianov et al. (2016), the globally averaged production rate (units of atoms/cm^2/s) by a solar proton event integrated over the duration of the event can then be expressed as:

$$Q_G = \frac{1}{4\pi}\int_h\int_\gamma\int_\lambda R\left(h, P_C\left(\gamma,\lambda\right)\right)\cdot dh\cdot d\gamma\cdot d\lambda, \quad (3)$$

with h being the atmospheric depth, γ the longitude and λ the latitude.

2.3. Geomagnetic Cut-Off Rigidities

Finally, to express the geomagnetic shielding that protects us from cosmic rays, we use Stoermer's rigidity cut-off for particles with a vertical incidence given by:

$$P_C = 14.9\left(\frac{M}{7.8}\right)\cos^4\lambda, \quad (4)$$

where M is the dipole moment in units of 10^{22} Am^2, with today's value set at 7.8. Assuming today's dipole moment, Equation 4 thus tells us that for a proton to enter the Earth's geomagnetic field at the equator, and with a vertical incidence, it requires a rigidity of 14.9 GV (Beer et al., 2012) which translates to a kinetic energy of ~14 GeV. The expression of Stoermer's cut-off energies that result from P_C for different values of M, relative to today, is plotted in Figure S1. We note here that other cut-off rigidity estimates such as modeled with for example, PLANETOCOSMICS (see Herbst, 2013) may lead to differences in the latitudinal production rates of cosmogenic radionuclides. The impact of these differences exceed the scope of this study though they should be addressed in the future.

2.4. Production by Galactic Cosmic Rays (GCRs)

Though a number of production rate time series spanning the Space Age already exist for ^{10}Be (e.g., Herbst, 2013; Poluianov et al., 2016; Webber et al., 2007; Usoskin et al., 2006), we present in Section 3 another such series using the assumptions and variables described below. We do this in order to relate the production caused by the 59 GLEs in a consistent manner with the production induced by galactic cosmic radiation which we will refer to herein as the "baseline" production. To do so, we use the relationship between the solar modulation function Φ, introduced by Gleeson and Axford (1968), and the local interstellar spectrum (LIS) the galactic cosmic ray spectrum prior to heliomagnetic inferences) model of Herbst et al. (2017). We note that several LIS estimates exist in the literature, leading to a comparable mean global production rate within 5% (Herbst et al., 2017). In addition to revealing large solar particle events at Earth, data from neutron monitors are also used to infer fluctuations in Φ. In the following, we take Φ for the period 1951–2016 CE from Usoskin et al. (2017). Finally, we assume a constant dipole moment $M = 7.8 \cdot 10^{22}$ Am^2 with a latitudinal rigidity cut-off as shown in Figure S1.

2.5. Simple Deposition Model

To infer depositional fluxes over latitudes where Greenland ice cores are located, we have used the parameterization from Heikkilä, Beer, and Feichter (2009), who conclude that 2% of ^{10}Be nuclides produced inside of the stratosphere are deposited within 1–2 years between 60-90N of latitude. In addition, 19% of nuclides produced within the troposphere of this Arctic latitudinal band are deposited in situ, whilst 5% of

the nuclides produced in the troposphere of the northern hemisphere's mid-latitudes (30–60N) are transported to and deposited at higher latitudes (see Table 3 in Heikkilä, Beer, & Feichter, 2009). Because we are eventually interested in the integral enhancement in the production and deposition rates of ^{10}Be and ^{36}Cl caused by SEP events, we simplify the transport delay with the following assumptions. We take the annual production in the mid-to-high latitude troposphere (30–90N) produced at year *n* to be deposited between 60-90N at year *n*, and the annual production in the stratosphere at year *n* to be deposited at year *n+1*. In the case of the deposition flux related to GCRs, we take the average tropopause height at each latitude and for every year as defined from the NCEP reanalysis data (https://psl.noaa.gov/data/gridded/data.ncep.reanalysis.html). As for the deposition flux related to SEPs, we use a dedicated tropopause height by considering the average height at each latitude for every month when a GLE occurred. We use a monthly resolved tropopause height for SEPs because SEP events are short-lived (few days) whereas we consider here annual averages for GCRs. For the purpose of this study, we extrapolate that the same transport/deposition parameterization applies for ^{36}Cl as it does for ^{10}Be. It is to be noted that no in-depth transport model exists to date for ^{36}Cl though it is believed that its mean residence time is similar to ^{10}Be (Heikkilä, Beer, Feichter, et al., 2009; Synal et al., 1990).

3. Production and Deposition Rates Throughout the Space Age

3.1. Production by Galactic Cosmic Rays (GCR)

The time series of the modeled global (i.e., averaged over the globe) annual atmospheric production rate of ^{10}Be, ^{14}C, and ^{36}Cl for the period 1951–2016 CE can be found in Figures 2a–c. As for the deposition fluxes, they can be found in Figure 2d for ^{10}Be and Figure 2e for ^{36}Cl.

In accordance with expectations (Figure 1) and with previous findings (Webber et al., 2007), the relative fluctuations in ^{10}Be and ^{36}Cl (and in ^{14}C) due to the 11-year cycle are virtually identical. In more detail, their global annual production rates (Figures 2a–2c) describe a quasi-11-year cycle with a mean peak (solar minimum) amplitude of +12% with respect to the mean, and a mean trough-to-peak (solar maximum to minimum) amplitude of +37.5% with respect to the minimum. For the investigated time period, we find a global mean ^{10}Be production rate of 2.9 10^{-2} atoms/cm^2/s, a global mean ^{36}Cl production rate of 2.5 10^{-3} atoms/cm^2/s and a global mean ^{14}C production rate of 1.6 atoms/cm^2/s. These values are in accordance to those given by Kovaltsov and Usoskin (2010), Herbst (2013), and Poluianov et al. (2016) for a mean solar modulation of $\Phi = 650$ MV. In contrast, many studies have reported a significantly lower average production rate for these radionuclides and for a similar time period. For instance, ^{10}Be values such as $\simeq$1.8 10^{-2} atoms/cm^2/s (Masarik & Beer, 1999; Webber et al., 2007) and ^{36}Cl values such as $\simeq$1.2 10^{-3} atoms/cm^2/s (Webber et al., 2007) or 1.9 10^{-3} atoms/cm^2/s (Masarik & Beer, 1999) have been previously reported. A further comparison of different global ^{10}Be production rates is provided in Table 1 of Kovaltsov and Usoskin (2010). Thus, there exists a discrepancy in the estimate of the global production rate of at least 50% which, nevertheless, can likely be traced back to the estimated cross section uncertainties given in Masarik and Beer (1999). It is also worth noting that Heikkilä (2007) anticipated that the production rate of the radionuclides simulated in Masarik and Beer (1999) is likely up to 50% too low, based on the analysis of observed and modeled deposition fluxes and surface air concentrations for ^{10}Be. Another disagreement concerns the mean ^{10}Be/^{36}Cl production ratio, which ranges from ca. 9.8 in Masarik and Beer (1999), meaning the global production rate of ^{10}Be is 9.8 times greater than that of ^{36}Cl, to about 15 in Webber et al. (2007). Poluianov et al. (2016) found a value of 11.6, which is used in this study.

3.2. Production by Solar Energetic Protons

In addition to showing the production rate induced by incident GCRs, Figure 2 also displays the contribution of the 59 GLEs analyzed in Raukunen et al. (2018) between 1956–2016 CE to the global production rate (a–c) and the resulting deposition flux at latitudes 60–90N (d, e) in the case of ^{10}Be and ^{36}Cl. We show the integrated effect of events that occurred throughout the same calendar year because we are mainly interested in the detectability and sensitivity of ^{10}Be and ^{36}Cl in annual ice core data.

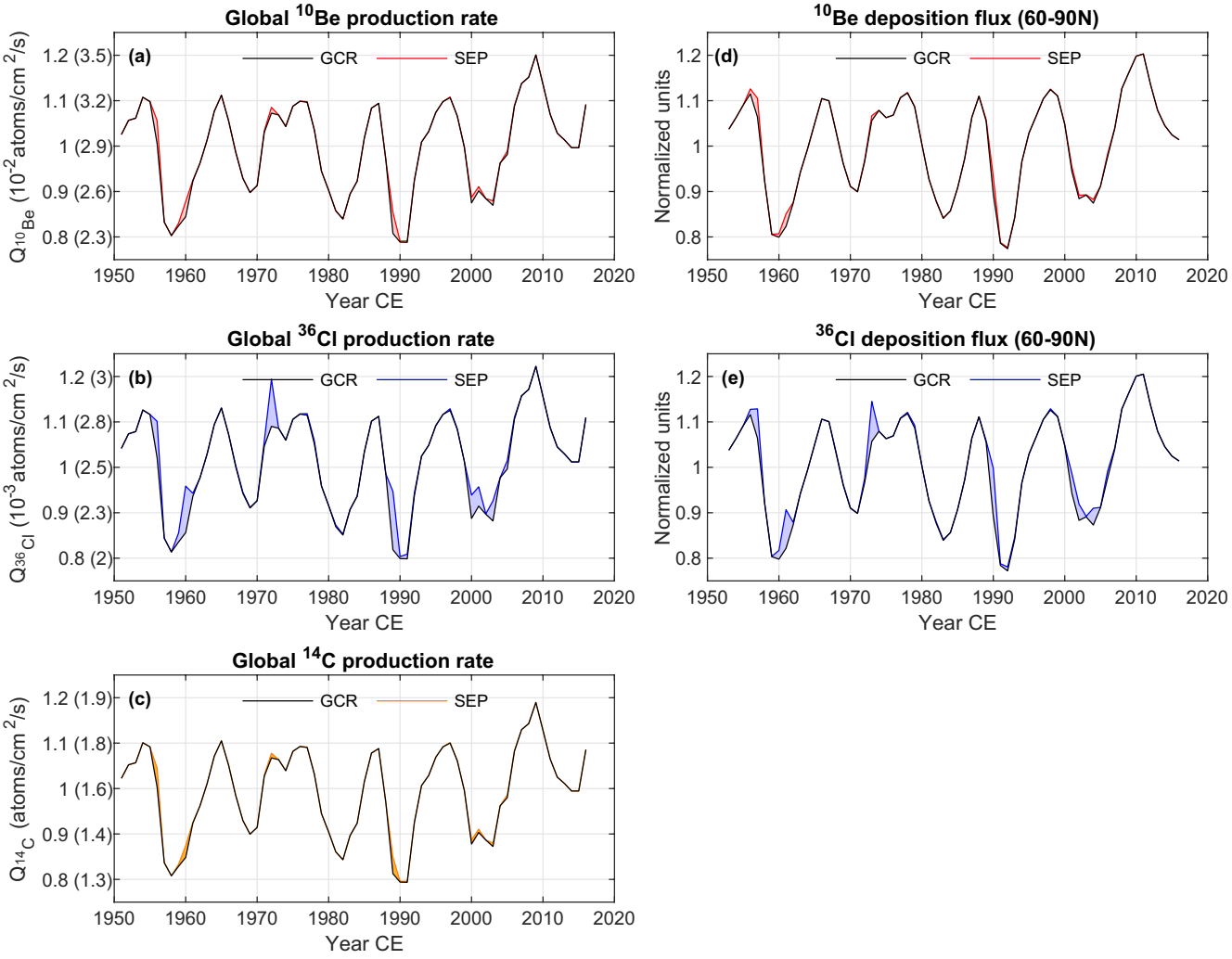

Figure 2. (a) The annual global production rate for ^{10}Be induced by galactic cosmic rays (GCRs) (black curve) and solar energetic particles (SEPs) (red shading). The *y*-axis units are normalized to the GCR baseline while the units in the brackets show the absolute value of the global production rate in atoms/cm^2/s. (b–c) Same as (a) but for ^{36}Cl and ^{14}C and with a blue and orange shading for SEP-related production. (d) The annual ^{10}Be deposition flux over latitudes 60–90N caused by production by GCRs (black curve) and SEPs (red shading) as well as transport as in Heikkilä, Beer, and Feichter (2009). (e) Same as (d) but for ^{36}Cl and with a blue shading for SEP-related production. (a) and (b) are an update from Webber et al. (2007) with more recent fluence spectra (Raukunen et al., 2018) and production functions (Poluianov et al., 2016).

3.2.1. Beryllium-10

Focusing on ^{10}Be first (Figures 2a and 2d), it can be seen that very few GLEs yield enough nuclides to increase the global annual production rate noticeably (red curve) relative to the baseline production rate caused by galactic cosmic rays (black curve). Of the years with notable events, we can mention 1956, 1960, and 1989 CE. These years witnessed the global ^{10}Be production rate being increased by about +5.2%, +4%, and +5.7%, respectively and with respect to the GCR baseline (black curves). When relating the additional production yielded by SEP events during these years to the mean ^{10}Be global production rate caused by GCRs during the Space Age instead (2.9 10^{-2} atoms/cm^2/s), we find increases of about +5.1%, +3.2%, and +4.6%. It is therefore not surprising that these GLEs have never been unequivocally linked to an increase in the ^{10}Be concentration of the many firn core ^{10}Be records available (e.g., Baroni et al., 2011; Beer et al., 1990; Berggren et al., 2009; Pedro et al., 2009; Zheng et al., 2020), in agreement with Herbst et al. (2015). A reappraisal and in-depth study of GLE no. 05 (1956 CE) was recently undertaken by Usoskin et al. (2020), wherein the fluence spectrum of the event was reevaluated. Based on this and on the production functions from Poluianov et al. (2016) coupled with a chemistry-climate model (SOCOL as in Sukhodolov et al., 2017),

Table 1
Global Annual Production Rate and Associated Increase Relative to the GCR Baseline (1951–2016) for ^{10}Be, ^{36}Cl and ^{14}C Caused by Selected GLEs Throughout 1951–2016

GLE no.	Date	[a]$Q^{10}Be$	[b]$X^{10}Be_{GCR}$	[c]$Q^{36}Cl$	[b]$X^{36}Cl_{GCR}$	$dQ^{14}C$	[b]$X^{14}C_{GCR}$
05	1956-02-28	1.47	+5.08%	2.00	+8.01%	6.73	+4.21%
07	1959-07-16	0.17	+0.58%	0.49	+1.97%	0.71	+0.44%
10	1960-11-12	0.62	+2.15%	1.64	+6.56%	2.70	+1.69%
11	1960-11-15	0.31	+1.05%	0.85	+3.39%	1.32	+0.83%
13	1961-07-18	0.06	+0.22%	0.16	+0.65%	0.26	+0.16%
23	1971-09-01	0.08	+0.26%	0.14	+0.57%	0.33	+0.20%
24	1972-08-04	0.34	+1.16%	2.48	+9.90%	1.50	+0.94%
41	1989-08-16	0.05	+0.18%	0.15	+0.59%	0.22	+0.14%
42	1989-09-29	0.36	+1.23%	0.80	+3.19%	1.55	+0.97%
43	1989-10-19	0.56	+1.92%	1.35	+5.42%	2.43	+1.52%
44	1989-10-22	0.16	+0.55%	0.50	+1.99%	0.67	+0.42%
45	1989-10-24	0.21	+0.73%	0.40	+1.60%	0.93	+0.58%
59	2000-07-14	0.35	+1.21%	1.29	+5.14%	1.49	+0.93%
62	2001-11-04	0.16	+0.57%	0.87	+3.47%	0.70	+0.44%
65	2003-10-28	0.19	+0.65%	0.82	+3.28%	0.81	+0.50%
69	2005-01-20	0.20	+0.67%	0.33	+1.31%	0.85	+0.53%

Abbreviations: GCR, galactic cosmic rays; GLE, ground-level enhancement.
[a]10^{-3} atoms/cm^2/s. [b]w.r.t. the GCR baseline during 1951–2016 CE. [c]10^{-4} atoms/cm^2/s. [d]10^{-2} atoms/cm^2/s.

they infer a similar figure with an increase of about 5%. On the other hand, Webber et al. (2007) estimated that GLE no. 05 increased the global production rate of ^{10}Be for the year 1956 by as much as +12%. This difference is likely to be caused by the 50% lower baseline (production by GCRs) in Webber et al. (2007) and may be attributed to the large uncertainties in the radionuclide production cross sections. In addition, even seasonally resolved (winter and summer) ^{10}Be measurements from a NEEM (Greenland) shallow core do not show a clear imprint of GLE no. 05 (see Zheng et al., 2020).

When atmospheric mixing, transport and deposition to the tropospheric latitudinal band 60–90N are considered (Heikkilä, Beer, & Feichter, 2009; Figures 2d and 2e), we notice that the SEP signal is slightly modulated. This is due to the combination of the delayed stratospheric fraction and also the varying tropopause height at the high latitudes (see different tropopause heights in Figure 3). Because we use a dedicated monthly tropopause (NCEP), the modeled deposition signal (the sum of the tropospheric and delayed stratospheric fractions) of certain GLEs may appear slightly larger or smaller than their global production rate counterparts. Overall however, the deposition flux signal of both the GCR and SEP components of both ^{10}Be and ^{36}Cl nuclides are strongly similar to their respective global production rate signal. The contribution of the main GLEs of the Space Age to the annual global production rate of ^{10}Be can be found in Table 1.

3.2.2. Chlorine-36

Expectedly, the global (Figure 2b) and polar (Figure 3) production rate of ^{36}Cl is relatively more enhanced by solar energetic protons than it is for ^{10}Be. Figures 3d and 3f indicate that the largest enhancement of SEP-induced ^{36}Cl nuclides, relative to the GCR production, comes from very high in the stratosphere (>32 km). There are multiple years when a GLE (or series of GLEs) can lead to a clearly visible increase in the global yearly production such as in 1956, 1960, 1972, 1989, 1990, 2001, and 2003. Since the 1950s, the GLE that induced the largest increase in ^{36}Cl production rate is GLE no. 24 (August 1972) with a ca. +10% contribution relative to the average GCR baseline followed by GLE no. 05 (1956) with a +8% increase. Unfortunately, the nuclear bomb tests carried out at sea during the 1950–70s resulted in a conspicuous anthropogenic peak in the ^{36}Cl concentrations of ice cores worldwide that is up to three orders of magnitude above the natural baseline (Heikkilä, Beer, Feichter, et al., 2009; Synal et al., 1990). This hinders us from identifying the signal

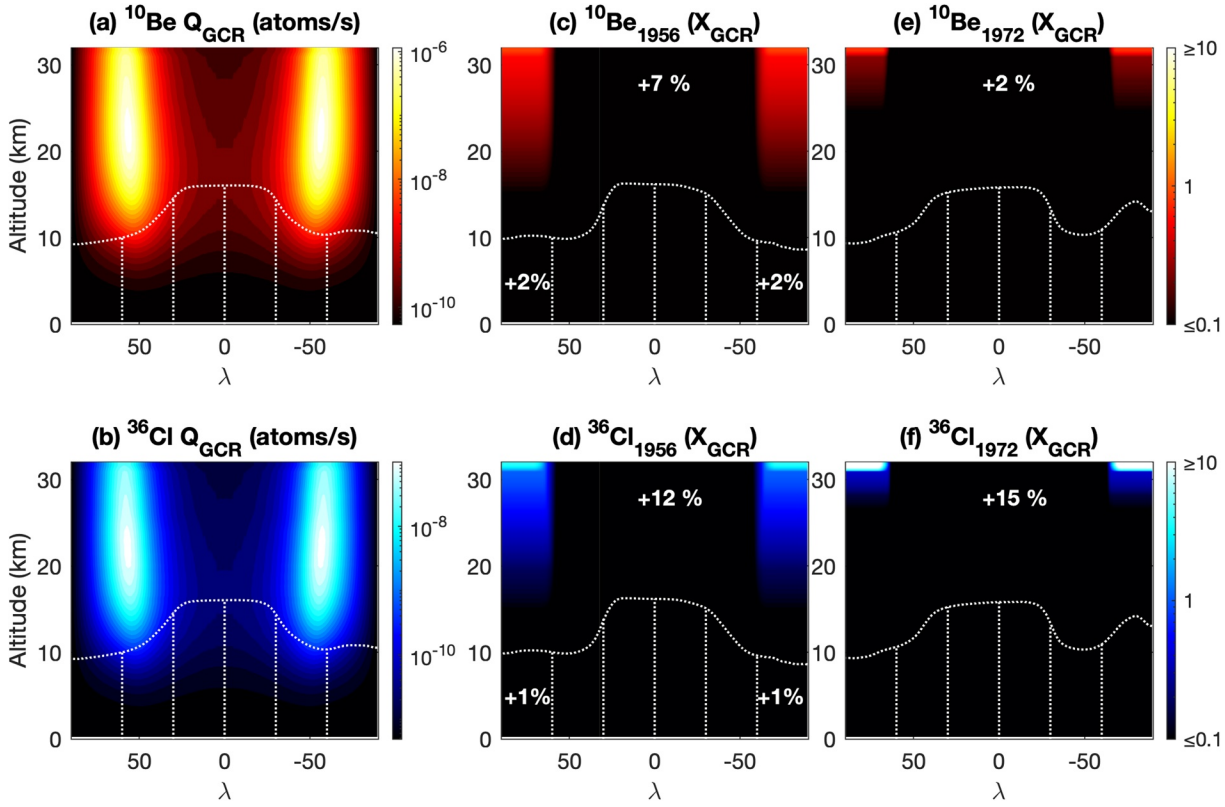

Figure 3. (a and b) The annual production rates of ^{10}Be (red) and ^{36}Cl (blue) in the atmospheric column and per latitude caused by galactic cosmic rays (GCRs) (Φ = 650MV). Note that each cell is latitudinally weighted. (c and d) The percentage increase in the production rate of ^{10}Be (red) and ^{36}Cl (blue), relative to the baseline production by GCRs (a), (b) caused by ground level enhancement (GLE) no. 05 in 1956 and for each latitude/altitude cell. (e), (f) Same as (c), (d) but for GLE no. 24 in 1972. The dashed lines delimit the different atmospheric boxes used to parameterize transport of the radionuclides to 60–90N, with the horizontal curves representing the tropopause. The tropopause for (a), (b) is the mean height for each latitude for the period 1950–2016 CE. The tropopause for (c), (d) and (e), (d) is taken as the mean height for each latitude during February 1956 CE and August 1972 CE, respectively.

of these GLEs in the global ^{36}Cl production rate. This is especially true for GLE no. 24 (August 1972) that occurred at the onset of a solar minimum, making it more readily visible (Figures 2b and 2e). If we assume the transport of ^{36}Cl nuclides to be akin to ^{10}Be, as well as consider the particularly large enhancement in the production rate due to SEPs in the stratosphere (Figure 3), then we find that GLEs no. 05 and 24 contributed to a comparable increase in the annual deposition flux over 60–90N, relative to the global annual production rate. Details on the contributions of the main GLEs to the global production rate of ^{36}Cl are also listed in Table 1.

3.2.3. Carbon-14

Though this study focuses on assessing the detectability of solar storms in ^{10}Be and ^{36}Cl concentrations from ice cores, Figure 2c also displays the global annual production rate of radiocarbon (^{14}C) throughout the Space Age. It can be seen that the signal of all GLEs that have occurred for the studied time period is very similar to ^{10}Be. As an example, GLE no. 05 has resulted in an enhancement of the annual global production rate of ^{14}C of +4.2% with respect to the mean global production rate of the Space Age whereas this number was +5.1% for ^{10}Be. Hence the sensitivity threshold for ^{14}C to SEPs is close to that of ^{10}Be. We note, however, that the ^{14}C yield function at energies below 200 MeV in Poluianov et al. (2016) is somewhat lower than other studies (see comparisons in Kovaltsov et al., 2012 or in Poluianov et al., 2016).

3.2.4. The ^{36}Cl/^{10}Be Ratio

Based on the finding that ^{10}Be and ^{36}Cl have different production rate sensitivities to solar energetic protons (Webber et al., 2007), it was suggested that the ^{36}Cl/^{10}Be ratio from ice core data can be used as a proxy for the spectral index of ancient solar storms (Mekhaldi et al., 2015). More specifically, the production of ^{10}Be

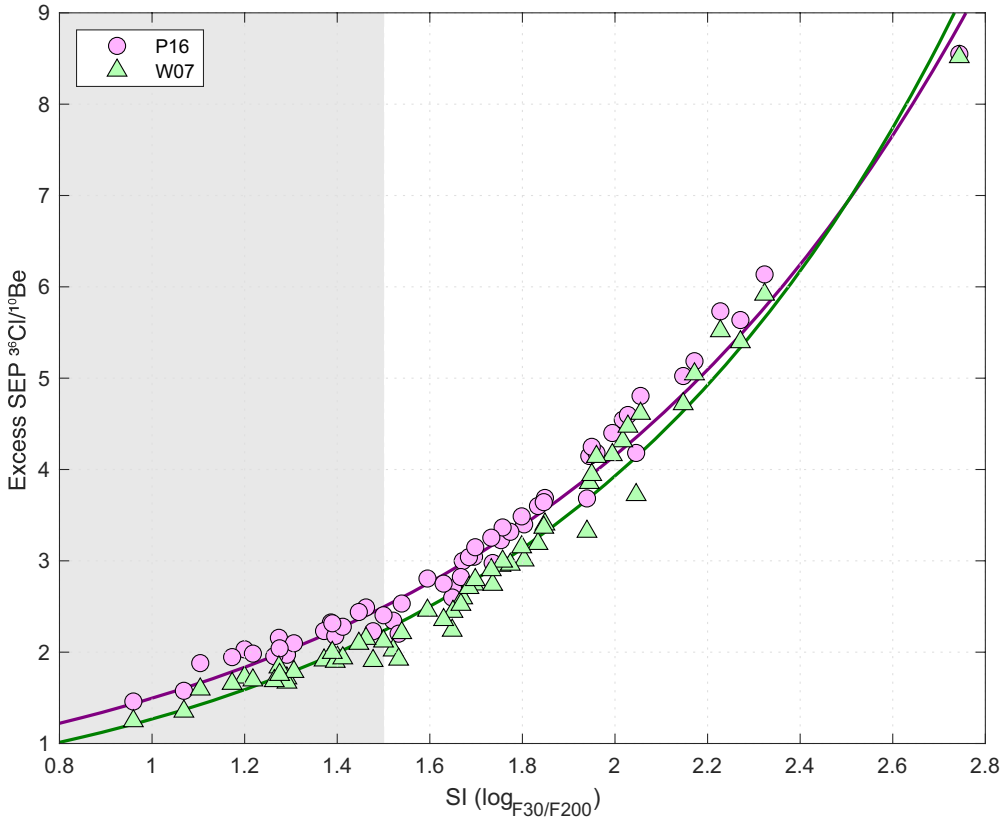

Figure 4. The excess solar energetic particles $^{36}Cl/^{10}Be$ ratio as a function of $SI_{30/200}$ for the 59 ground level enhancement analyzed in Raukunen et al. (2018). Magenta dots were obtained by using the yield functions from Poluianov et al. (2016) while the green triangles were obtained by using the yield functions from Webber et al. (2007).

by SEPs peaks for incident protons at about 200 MeV (depending on the energy spectrum), whereas the production of ^{36}Cl peaks for incident SEPs at about 30 MeV (Webber et al., 2007). Therefore, the $^{36}Cl/^{10}Be$ ratio will be higher (lower) for softer (harder) spectra. Figure 4 shows the exponential fit between the ratio and the spectral index $SI_{30/200}$. It can be inferred that most SEP events would lead to a two-to-threefold increase in the production rate of ^{36}Cl (and ice-core concentration) relative to the increase in ^{10}Be (both relative to their respective GCR baselines). As a matter of fact, even the bulk of hard events ($SI < 1.5$ delimited in Figure 4 by a gray rectangle) would result in a doubling of the ratio of the $^{36}Cl/^{10}Be$ excess production due to SEPs compared to the $^{36}Cl/^{10}Be$ baseline from GCRs (henceforth the excess SEP $^{36}Cl/^{10}Be$ ratio). As for events characterized by particularly soft spectra ($SI > 2$), they would produce about 4–6 times more ^{36}Cl relative to its GCR baseline than ^{10}Be relative to its GCR baseline. On the other end of the hardness spectrum, the record high F_{30} solar proton event (GLE no. 24) that was exceptionally soft indicates an excess SEP $^{36}Cl/^{10}Be$ ratio (relative to the GCR-baseline ratio) greater than 8. Doing the same exercise but using the yield functions from Webber et al. (2007) and relative to their estimate of the mean global production of ^{10}Be and ^{36}Cl, we find a very similar result (green curve in Figure 4). This shows that although many uncertainties prevail when modeling the radionuclide production induced by SEP events, the excess SEP $^{36}Cl/^{10}Be$ ratio can be regarded as a sound proxy of the spectral index. Based on the yield functions from Poluianov et al. (2016) and the fluence spectra presented in Raukunen et al. (2018), we can thus fit the following relationship:

$$\left(^{36}\mathrm{Cl}\ /\ ^{10}\mathrm{Be}\right)_{\mathrm{excess}} = 0.54\left(e^{1.02\mathrm{SI}}\right). \quad (5)$$

3.2.5. Geomagnetic and Solar Modulation Effects

Ice cores provide us with the opportunity of obtaining highly resolved ^{10}Be data throughout and beyond the Holocene that spans the past 11,650 years. During this time period, both solar modulation (e.g., Steinhilber et al., 2012; Vonmoos et al., 2006) and the dipole moment (e.g., Knudsen et al., 2008; Nilsson et al., 2014)

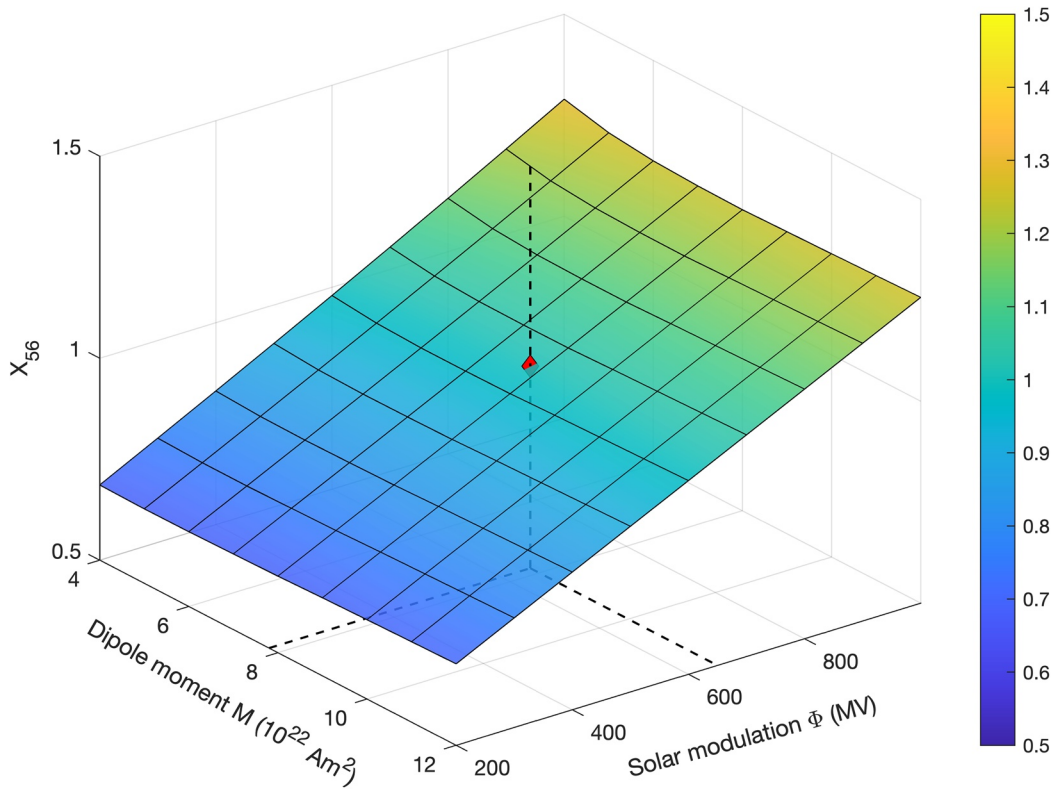

Figure 5. Percentage change in the annual global production-rate increase caused by ground level enhancement(GLE) no. 05, relative to the galactic cosmic rays baseline, as a function of Φ and M. For Φ values ranging from 200 to 1000 MV, the relative increase in the global production rate caused by for example, GLE no. 05, would vary by up to ±30%. The red dot indicates today's Φ and M. The same dependencies exist for ^{14}C and ^{36}Cl.

have varied significantly. These changes affect the detectability of the SEP signal in different ways. This is illustrated in Figure 5 that displays the percentage change in the relative increase due to GLE no. 05 compared to the GCR induced production as a function of Φ and M. It can be inferred that changes in the dipole moment in the range of what has been reported for the Holocene lead to no significant change in the relative increase of the production rate of ^{10}Be caused by GLE no. 05. This is because variations in the magnetic shielding affect both SEPs and GCRs. We stress, however, that the absolute production rate due to SEPs would vary greatly with changes in the dipole moment by changing the area of the latitudinal band of low cut-off rigidity values (Figure S1). This is especially true for dipole moment vaIues below $4 \cdot 10^{22}$ Am^2. It can also be inferred that the solar modulation has a large impact on the relative increase associated with SEP events. This is because solar modulation affects the GCR baseline while having no effect on the SEP-related production. This leads to a reduced (increased) relative SEP enhancement with a lower (higher) Φ-value. For Φ values ranging from 200 to 1000 MV, the relative increase in the global production rate caused by for example, GLE no. 05, would vary by up to ±30% (see Figure 5).

3.3. Potential Contribution of Solar Energetic He-Particles

Although SEP events mainly accelerate protons, a smaller fraction of heavier particles are also accelerated such as He particles. This was for instance observed during the "Halloween storms" in 2003 with integrated abundances leading to H/He ratios ranging between 8.7 and 30.2 for nucleon energies between 0.1 and 100 MeV (Mewaldt et al., 2005). These values are relatively close to those measured from solar wind (Grevesse & Sauval, 1998; von Steiger et al., 2000) and from the abundance ratio determined for the outer corona with a value of 19.2 ± 10% (Laming & Feldman, 2001). Because no systematic He fluence spectra exist for each of the 59 GLEs studied here we multiplied the differential spectra for protons by a factor of 0.052 (see example in Figure S2). For ^{10}Be this leads to an enhanced global production rate due to these GLEs

Table 2
Estimated Uncertainties of Different Parameters Involved

Uncertainty	Estimated uncertainty
Accelerator mass spectrometry error	±5%
Fluence spectra	±26%
Contribution of He-particles (for ^{36}Cl)	+3.5%
Contribution of He-particles (for ^{10}Be)	+12%
^{10}Be yield functions (at SEP energies)	±50%
Long-term solar modulation	±30%
Ice core data noise	±20%
Mean production rate (by GCRs)	±50%

ranging between +8% to +24% (mean: +12%), with respect to the yearly increase due to solar energetic protons alone. We see an increasing contribution of He-particles with "softness" of the GLEs (Figure S2) that we interpret as the growing difference in cut-off rigidities between protons and He-particles (Figure S2) with softer spectra. The overall contribution of He-particles to the global production rate of ^{36}Cl caused by GLEs is lower than that of ^{10}Be, with values ranging between +2% to +5% (mean: 3.5%). We interpret this as the expression of the importance of the resonance of the target nuclei ^{40}Ar in interaction with protons at ∼25 MeV (Webber et al., 2007) for the production rate of ^{36}Cl. However, the H/He abundance ratio is highly variable not only for each SEP event, but also as a function of the energy of the nucleons (Mewaldt et al., 2005). In addition, the H/He abundance ratio may increase with energy (Mewaldt et al., 2005), implying a possibly diminished relevance for the contribution of He-particles to the global production rate of radionuclides caused by SEP events. In consequence, we decide not to include their contribution for this study as it may introduce additional uncertainties.

3.4. Quantifiable Uncertainties

All main known uncertainties affecting the quantification of extreme SEP events from ice core data discussed here are reported in Table 2. This includes the small uncertainties related to accelerator mass spectrometry measurements of radionuclides, the influence of the varying solar modulation on the baseline value (Figure 5) and the uncertainty in the yield functions at energies relevant for production by SEPs. The latter was estimated by looking at the difference in the absolute production rate in ^{10}Be induced by GLE no. 05 using the yield functions from Webber et al. (2007) relative to using those from Poluianov et al. (2016). Uncertainties related to the fluence spectra of the 59 GLEs (Raukunen et al., 2018) reach about ±26% for protons with energies above 30 and 200 MeV leading to an uncertainty in the global production rate of radionuclides due to these events of also ±26%. Note that this uncertainty does not bear relevance for the estimate of the fluence of the pre-industrial extreme events. Finally, the noise inherent to ice core data is discussed in the following section.

4. The Imprint of the 774/5 CE Event on ^{10}Be Concentrations

Figure 6 displays the published ^{10}Be concentration data from five ice records cored in Greenland (magenta) and Antarctica (green) that span the extreme solar event of 774/5 CE. The 774/5 CE event represents the largest pre-industrial solar storm of the three discovered thus far and so, it is also the best studied with many Δ^{14}C records from tree rings (e.g., Büngten et al., 2018; Güttler et al., 2015; Miyake et al., 2012; Uusitalo et al., 2018) and ^{10}Be data from ice cores (Mekhaldi et al., 2015; Miyake et al., 2015; Sigl et al., 2015). The ^{10}Be data set plotted in Figure 6 thus encompasses five (quasi-) annual records of ^{10}Be concentrations during the event but also preceding and following it. Some of the records (NEEM, NGRIP, WAIS) span more than two decades. In consequence we can study not only the shape of the ^{10}Be peak itself, but we can also gauge the mean signal-to-noise ratio of the peak by considering ice cores from a wide array of localities.

All data from Figure 6 have been normalized to their mean, excluding the peak taken here as data points rising above 3σ of the shown period. In doing so, we can compare the relative changes common to all five ice cores that show a similar standard deviation of ca. 20% of the mean (Table S1). The Tunu and Dome Fuji ice cores are characterized by a lower accumulation rate (Fujita et al., 2011; Maselli et al., 2017) and show a somewhat greater standard deviation of about 25%. These two ice core records reveal a smaller amplitude of the ^{10}Be peak (A_{peak} = highest value - baseline) caused by the 774/5 solar storm event, compared to the NEEM, NGRIP and WAIS ice cores (Table S1). The time distribution of ^{10}Be at 774/5 CE also differs from the simplified production-transport model used here. In fact, the event left an imprint on the ^{10}Be concentration of ice cores lasting from <2 years to three years. This likely is the consequence of the combination of the many processes that take place upon production in the polar stratosphere (Figures 3c–3f) though we cannot rule out the possibility of multiple events. Of these we can mention stratospheric transport with a

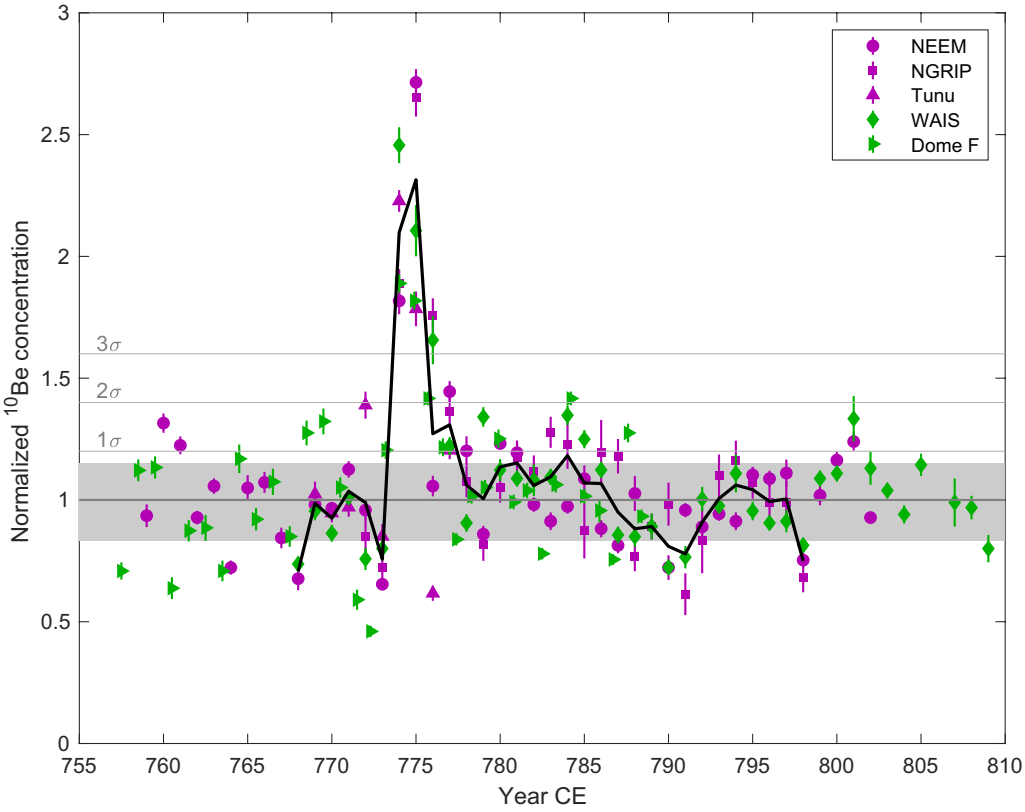

Figure 6. The ^{10}Be concentration data from 3 ice cores from Greenland (magenta) and 2 ice cores from Antarctica (green). All five records were normalized to their mean, excluding the peak and the black curve represents a stack of these ^{10}Be records. The three lines show the 1, 2, and 3σ levels as in Table S1. The gray envelope encompasses the variability expected from the 11-year cycle, inferred from Figures 2a and 2d.

stratospheric residence time of about 1–2 years (Heikkilä, Beer, & Feichter, 2009), stratosphere-troposphere exchanges that are modulated seasonally (e.g., Škerlak et al., 2014; Stohl et al., 2003, Zheng et al., 2020), depositional and post-depositional effects such as wind-blown snow (Pedro et al., 2006) and finally, the stochastic process of human sampling and handling. Therefore, the time-integrated peak ($\int_{peak}$) is a better representation of the impact of the 774/5 event on the ^{10}Be production which was of a factor of about 2.6 times the GCR-related baseline (Table S1). This factor estimate is raised to 3 when the more uncertain (greater standard deviation) Tunu and Dome Fuji ice cores are not considered. Table S1 also relates $\int_{peak}$ to A_{peak} of each ice cores. In doing so, it can be seen that in general, about half (0.54) of $\int_{peak}$ is expressed within the peak amplitude for quasi-annual samples. For such resolution, this value agrees with a residence time distribution *F(t)* with a mean τ of 1–2 years (Heikkilä et al., 2008; Raisbeck et al., 1981) assuming that

$$F(t) = e^{-t/\tau}. \quad (6)$$

This means that for a SEP event to leave an imprint at the 3σ level in ice core ^{10}Be data, its time-integrated production (or associated deposition flux) shall exceed the baseline production by a factor of *ca.* 4.4σ (1.46 · 3σ). To put this result into perspective, this in turn implicates that a SEP event with a spectral hardness such as GLE no. 05 may be robustly detectable in annual ^{10}Be data if the deposition flux it induced exceeds a coefficient X_{05} of 17 (4.4σ/5.2%), that is, the event would have needed to be 17 times larger. Usoskin et al. (2020) pointed out that by combining several ice cores, a smaller coefficient X_{05} may be sufficient to achieve detection. Unfortunately, there exist at present only two short periods of time where more than two annual ^{10}Be records coexist i.e., the Space Age (1950–Present) and the 774/5 CE event shown in Figure 6.

5. The Detectability of Extreme Solar Storms in ^{10}Be and ^{36}Cl Data

5.1. Methodology

In Section 3, we have modeled the global annual production rate and the annual deposition flux at high northern latitudes for ^{10}Be and ^{36}Cl that can be credited to the 59 largest GLEs since the 1950s. This has shown that the integrated signal of solar storms in ice cores likely mirrors that of the global production rate. In Section 4, we have shown that the signature of the 774/5 CE event in ice-core ^{10}Be data likely lasted for an average of three years. We justified this long-lasting signature by the combined effects of the residence time distribution due to atmospheric transport, in addition to (post-) depositional processes and sampling approximations. As a result, a peak amplitude of about half the integrated production enhancement caused by a SEP event can be expected with annual samples (Table S1). We extrapolate that this result holds true for ^{36}Cl that has a similar stratospheric residence time of 1–2 years (Heikkilä, Beer, Feichter, et al., 2009; Synal et al., 1990). Its main difference in comparison to ^{10}Be concerns its potential for back-diffusion within the snowpack (Delmas et al., 2004) caused by its gaseous form ($H^{36}Cl$), though this process is not expected to be an important uncertainty for ^{36}Cl records from localities with sufficiently high accumulation rates (Delmas et al., 2004; Pivot et al., 2019) which is the case in Greenland. Furthermore, we have inferred that a SEP event (or any other cosmic-ray event) must yield an enhancement in the global annual production rate of ^{10}Be (and ^{36}Cl) of at least 4.4σ the GCR-related baseline for its signature to be identified reliably (at the 3σ level) in annual data in a single ice core record. Taken together, we can use these estimates to test the F_{30} necessary for SEP events of different hardness to increase the annual production rate in ^{10}Be and ^{36}Cl above this detection limit. For this exercise, we assume that the noise in annual ^{36}Cl data is similar to ^{10}Be although no such highly resolved data have been published to date, at the exception of the period 1950–1990 CE that covers the anthropogenic releases from nuclear bomb testing. Because the influence of changes in the dipole moment only affects the relative production enhancement marginally (Figure 5), we consider today's dipole moment $M = 7.8 \cdot 10^{22}$ Am^2 for the subsequent discussion. As for solar modulation, we take $\Phi = 650$ MV which corresponds to the mean value throughout the Space Age (for Φ estimated from neutron monitors in Usoskin et al., 2017).

Figure 7 shows the enhancement coefficient (X_{GCR}) of the global annual production rate of ^{10}Be (a) and ^{36}Cl (b) that a SEP event with a spectral hardness such as the 59 GLEs analyzed in Raukunen et al. (2018) would incur as a function of a F_{30} ranging from 10^9 to $5 \cdot 10^{11}$ protons/cm^2. The spectral indexes ($SI_{30/200}$) used here range from 0.97 to 2.74 (Cliver et al., 2020; Figure 4) with values greater than 1.5 considered as soft spectra. As references, we can cite the benchmark hard GLE no. 05 (Feb. 1956) with a $SI_{30/200}$ of 1.07 and the soft GLE no. 24 (Aug. 1972) with a $SI_{30/200}$ of 2.74 (Cliver et al., 2020). The former event holds the record for the largest F_{200} ever directly measured while the latter event holds the record for the largest F_{30}. Different levels of the noise and variability present in ice core data (illustrated in Figure 6) are denoted with horizontal dashed lines and have been multiplied by 1.46 to take into account the effect of the residence time distribution discussed in the previous section. The gray band encompasses the variability that is expected from the 11-year solar modulation, inferred from Figure 2. In consequence, the intercept of each curve with the 3σ line is considered as the enhancement coefficient of the annual global production rate (y-axis) caused by the corresponding F_{30} (x-axis) necessary for each of the 59 different spectral hardness examples to be identified in one annual ^{10}Be (a) and ^{36}Cl (b) ice core record.

5.2. Analysis

The detectability test described above and summarized in Figure 7 confirms that ^{36}Cl is better suited than ^{10}Be to detect the signature of solar proton events in ice cores with annual samples. This is strikingly illustrated in the figure with the bulk of the ^{36}Cl curves rising above 3σ at significantly lower F_{30} values than the bulk of the ^{10}Be curves. In fact, an event with a spectral index such as GLE no. 05 and GLE no. 08 in the range of SI = 1 and with a theoretical F_{30} in the vicinity to GLE no. 24 (ca. $7.8 \cdot 10^9$ protons/cm^2, Raukunen et al., 2018; Cliver et al., 2020) could possibly be identified at the 2σ level in annual ^{36}Cl data. In addition, the difference in detectability between ^{36}Cl and ^{10}Be increases with $SI_{30/200}$, that is to say with increasing softness. Figure 7 thus emphasizes that annual ^{10}Be data can likely only register particularly hard events that represent only a minority of all GLEs known to date (see Figure 4), as was the case with the ancient events

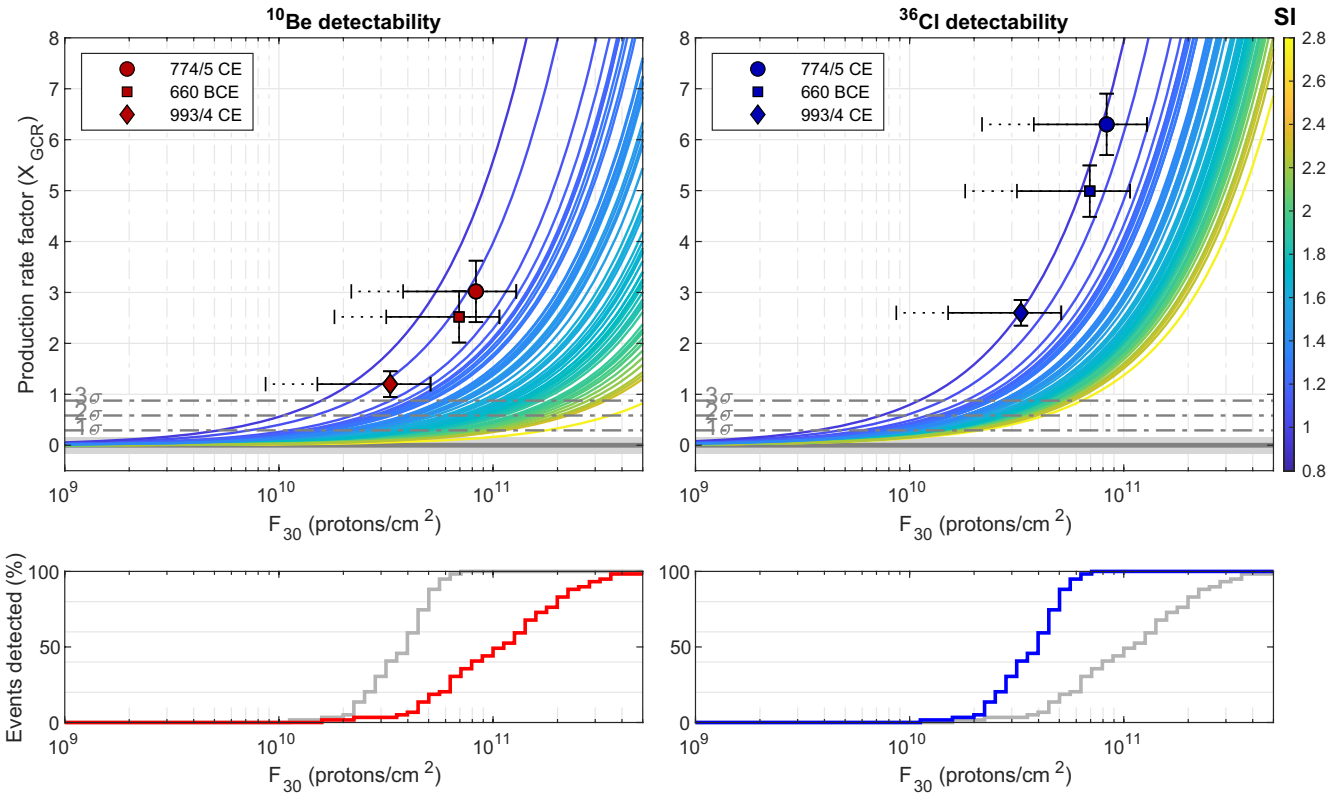

Figure 7. Detectability test of ^{10}Be (left panels) and ^{36}Cl (right panels) produced by solar energetic particles with 59 different $SI_{30/200}$ (see colorbar). (Top panels) The global production rate enhancement factor of each 59 ground level enhancement scenarios and relative to the galactic cosmic rays baseline (X_{GCR}) as a function of F_{30}. The 1-to-3σ significance levels are denoted with horizontal dashed lines. The estimated F_{30} for the three historical events of 993/4 CE, 774/5 CE, and 660 BCE are plotted with corresponding uncertainties. See text for details. (Bottom panels) The fraction of detected events as a function of F_{30} for ^{10}Be (red) and ^{36}Cl (blue). The gray curves represent ^{36}Cl in the bottom-left panel and ^{10}Be in the bottom-right panel.

of 774/5 CE, 993/4 CE, and 660 BCE (Mekhaldi et al., 2015; Miyake et al., 2015; O'Hare et al., 2019). This is evidenced by a clustering in the ^{10}Be curves with the two extremely hard GLEs no. 05 and 08 ($SI_{30/200}$ = 1.07 and 0.96, Cliver et al., 2020) resulting in ^{10}Be peaks that rise above 3σ for $F_{30} > 2 \cdot 10^{10}$ protons.cm^{-2} whereas the bulk of the other 57 GLE scenarios with SI above about 2 would require a F_{30} with, at least, an additional order of magnitude to achieve detectability.

The enhancement coefficient in ^{10}Be and ^{36}Cl measured in ice cores for the three historical events at 993/4 CE, 774/5 CE (Mekhaldi et al., 2015) and 660 BCE (O'Hare et al., 2019) are also plotted in Figure 7. Their corresponding F_{30} was calculated with the assumptions detailed in section 4, the data presented in Figure 6 and Table S1 in the case of 774/5 CE and the data from Mekhaldi et al. (2015) and O'Hare et al. (2019) for 993/4 CE and 660 BCE. As for the GCR baseline, we take the mean global annual production rate shown in Figure 2 for 1951–2016 CE corresponding to those shown in Poluianov et al. (2016). This gives us F_{30} values of 3.3 ± 1.8, 8.3 ± 4.5 and 6.9 ± 3.8 10^{10} protons/cm^2 for 993/4, 774/5 CE and 660 BCE, respectively. The errors were calculated using uncertainty propagation of the values listed in Table 2 with the larger dotted error bars in Figures 7a and 7b reflecting the 50% difference in estimates of the global mean production rate from various studies, as discussed earlier. By adjusting the GCR baseline for Φ during these different periods (see e.g., Steinhilber et al., 2012; Vonmoos et al., 2006) accordingly to Figure 4, F_{30} is raised to ca. 4.1, 9.4, and 7.7 10^{10} protons/cm^2 for the 993/4 CE, 774/5 CE and 660 BCE events, respectively. We stress that these values are tentative and that there exists different Φ estimates for these periods. In the case of 774/5 CE, the large number of Δ^{14}C data and carbon cycle modeling allowed Büngten et al. (2018) to infer an absolute ^{14}C production of 9.6 ± 0.5 · 10^{26} atoms which corresponds to a global annual production rate of 5.96 ± 0.3 atoms/cm^2/s. To explain this figure and considering the somewhat stronger dipole moment during the 8th century, a F_{30} of 1.38 ± 0.07 · 10^{11} protons/cm^2 is then required. However, this F_{30} can be reduced if the yield

functions from Kovaltsov et al. (2012) or Castagnoli and Lal (1980) are considered, for instance. A comparison of different ^{14}C yield functions can be found in Kovaltsov et al. (2012) and Poluianov et al. (2016) showing that the latter is lowest within the energy range corresponding to solar energetic protons, illustrating the uncertainties of inferring the magnitude of ancient events that arises from the production rate models used.

Because we use the energy spectrum of GLE no. 05 for all three events as a reference, they plot atop the ^{10}Be curve corresponding to the GLE in question in Figure 7. It should be clarified that the 5–6-year resolution of the ^{36}Cl measurements from the GRIP record (Wagner et al., 2000; Mekhaldi et al., 2015; O'Hare et al., 2019) and thereby the larger uncertainty relative to the ^{10}Be increase does not permit us to pinpoint exactly the spectral shape of the events. Rather, we can confidently conclude that they were particularly hard akin to a range of $SI_{30/200}$ colored in dark shades of blue in Figure 7 ($SI < 1.5$). Thus, the possible F_{30} of these events can be reduced are we to assume a slightly harder energy spectrum such as GLE no. 08 (05-04-1960). On the other hand, the opposite applies for a slightly softer spectrum. We parallelly justify why the events do not plot atop the ^{36}Cl curve corresponding to GLE no. 05 through the uncertainty in the $^{36}Cl/^{10}Be$ ratio and thereby in the estimated $SI_{30/200}$. It is nonetheless useful to observe that the 993/4 CE event led to an increase in ^{36}Cl that was over 9σ (coefficient of 2.6 in Mekhaldi et al., 2015). Meanwhile, the peak in ^{10}Be just barely rose above the 3σ threshold level (Figure 7a). In other words, even a SEP event as extreme and hard as the 993/4 CE event is difficult to identify in annual ^{10}Be data alone and without the prior knowledge from high resolution $\Delta^{14}C$ data from tree rings which do not suffer from depositional noise like ^{10}Be. By contrast, the 993/4 CE event was easily identified in the lower resolution ^{36}Cl data (ca. 6 years) from the GRIP ice core (Mekhaldi et al., 2015). This also indicates that Figures 7b and 7d is also relevant for ^{36}Cl with a lower resolution such as 5 years. This is due to the fact that a lower resolution would smooth the peak but also the noise and variance surrounding the peak.

5.3. Implications

The bottom panels in Figure 7 describe the fraction of detectable events in ice core ^{10}Be (left) and ^{36}Cl (right) data as a function of F_{30}, based on the results from the top panels. This assumes that the spectral shape ($SI_{30/200}$) distribution of potential SEP events with extreme F_{30} values above 10^{10} protons/cm^2 is analogous to the $SI_{30/200}$ distribution of the observed GLEs from the Space Age. Figure 7d indicates that, in the case of ^{36}Cl, all simulated events/spectra with $F_{30} > 6 \cdot 10^{10}$ protons/cm^2 (i.e., the 660 BCE event) may be identified in annual ice core data. However, only about one third of the events also lead to a ^{10}Be increase above 3σ. This corresponds to the percentage of events with $SI_{30/200} < 1.47$, that is to say only hard events. Similarly, are we to take the F_{30} value of the 993/4 CE event as a yardstick for past extreme events, then we find that only about 3% of events from the 59 $SI_{30/200}$ examples used here may be identified, corresponding to the spectra of GLE no. 05 and GLE no. 08. In comparison, all "hard GLEs" (30% of the 59 GLEs) would be observed at the 3σ level in ^{36}Cl data.

These results imply that by relying on annually resolved ^{10}Be (and ^{14}C) to document past extreme SEP events, their occurrence rate estimate is likely relating to only a small population of potential events (i.e., hard spectra). As a counterargument to this, we can mention that Asvestari et al. (2016) have shown that a hard spectrum can be assumed for all extreme GLE events, including those studied in cosmogenic radionuclide data. While this argument holds true for GLE detection rather than F_{30}, Figure 7 suggests that ^{36}Cl does not follow this rule in that its production is sensitive enough to SEPs from soft events to leave their imprint on the concentration of ice core records. In that light, it is furthermore important to be mindful that the GLEs associated with the 10 largest F_{30} recorded since the 1950s were all soft ($SI_{30/200} > 1.5$) with the exception of GLE no. 05 (Cliver et al., 2020). Therefore, ^{36}Cl has the potential to provide a more accurate account of SEP events with extreme F_{30} prior to the 1950s that would likely be impactful on spacecraft technologies, were they to occur today. Finally, we note that soft events tend to originate from the central meridian of the Sun (Cliver et al., 2020) and are thereby often associated with large CMEs. This means that ^{36}Cl may also serve as an indirect proxy for large geomagnetic storms from the past.

6. Conclusions

We have modeled the global annual production rate of ^{10}Be, ^{14}C, and ^{36}Cl as well as their expected annual deposition flux at high latitudes (for ^{10}Be and ^{36}Cl) induced by solar energetic protons (SEP) associated with 59 ground level events (GLEs) between 1956-2012 CE. This showed that no GLEs of the past 70 years are likely to be detected in ice cores, in agreement with Herbst et al. (2015). By considering these results as well as the noise and variability present in ice core data, we have performed a detectability test of the signal of extreme solar storms embedded in ^{10}Be and ^{36}Cl nuclides in ice cores. We found that ^{10}Be (and thus ^{14}C) is suitable to detect only hard events ($SI_{30/200} < 1.5$) that represent a minority in the population of the 59 GLEs analyzed here. Contrary to this, the production rate of ^{36}Cl is sensitive enough to SEPs so that any extreme solar event (similar in F_{30} to the three ancient events) may be detected in ice core, regardless of the spectral shape. This implies that the probability of extreme solar storms to hit Earth may be greater than ^{10}Be and ^{14}C data imply. In addition, ^{36}Cl may serve as an indirect proxy for the occurrence of large geomagnetic storms because of the similar relationship between $SI_{30/200}$ and CME source distribution with solar longitude. Hence it will be important in the future to measure additional ^{36}Cl data from ice cores in order to better ascertain the threat that large solar and geomagnetic storms represent.

Data Availability Statement

Datasets for this research and used for the production model detailed in this study are included in this paper (and its supplementary information): Poluianov et al. (2016); as well as in this paper: Raukunen et al. (2018). A version of Table 1 including all 59 GLEs and different dipole moment values is available as supplemental information and will be made available at https://doi.org/10.17632/z9vwfvdfgn.1.

Acknowledgments
We thank Ed Cliver for stimulating and insightful discussions. Stepan Poluianov is also acknowledged for his insight on the production functions. This work was supported by a grant from the Swedish Research Council to R. Muschele (DNR2013-8421). F. Adolphi acknowledges funding by the Helmholtz Association (VH-NG-1501). F. Mekhaldi acknowledges funding from the Swedish Research Council (2020-00420). K. Herbst acknowledges the support of the DFG priority program SPP 1992 "Exploring the Diversity of Extrasolar Planets (HE 8392/1-1)" and thank ISSI Team 464 for fruitful discussion.

References

Asvestari, E., Willamo, T., Gil, A., Usoskin, I. G., Kovaltsov, G. A., Mikhailov, V. V., & Mayorov, A. (2016). Analysis of Ground Level Enhancements (GLE): Extreme solar energetic particle events have hard spectra. *Advances in Space Research*, *60*(4), 781–787. https://doi.org/10.1016/j.asr.2016.08.043

Band, D., Matteson, J., Ford, L., Schaefer, B., Palmer, D., Teegarden, B., et al. (1993). BATSE observations of gamma-ray burst spectra. I-Spectral diversity. *The Astrophysical Journal*, *413*, 281–292. https://doi.org/10.1086/172995

Bard, E., Raisbeck, G. M., Yiou, F., & Jouzel, J. (1997). Solar modulation of cosmogenic nuclide production over the last millennium: Comparison between 14C and 10Be records. *Earth and Planetary Science Letters*, *150*(3–4), 453–462. https://doi.org/10.1016/s0012-821x(97)00082-4

Baroni, M., Bard, E., Petit, J. R., Magand, O., & Bourlès, D. (2011). Volcanic and solar activity, and atmospheric circulation influences on cosmogenic ^{10}Be fallout at Vostok and Concordia (Antarctica) over the last 60years. *Geochimica et Cosmochimica Acta*, *75*(22), 7132–7145. https://doi.org/10.1016/j.gca.2011.09.002

Beer, J., Blinov, A., Bonani, G., Finkel, R. C., Hofmann, H. J., Lehmann, B., et al. (1990). Use of ^{10}Be in polar ice to trace the 11-year cycle of solar activity. *Nature*, *347*(6289), 164–166. https://doi.org/10.1038/347164a0

Beer, J., McCracken, K., & von Steiger, R. (2012). *Cosmogenic radionuclides: Theory and applications in the terrestrial and space environments*. Springer. https://doi.org/10.1007/978-3-642-14651-0

Beer, J., Tobias, S., & Weiss, N. (1998). An active Sun throughout the Maunder minimum. *Solar Physics*, *181*(1), 237–249. https://doi.org/10.1023/A:1005026001784

Berggren, A.-M., Beer, J., Possnert, G., Aldahan, A., Kubik, P., Christl, M., et al. (2009). A 600-year annual ^{10}Be record from the NGRIP ice core, Greenland. *Geophysical Research Letters*, *36*(11), L11801. https://doi.org/10.1029/2009GL038004

Büntgen, U., Wacker, L., Galván, J. D., Arnold, S., Arseneault, D., Baillie, M., et al. (2018). Tree rings reveal globally coherent signature of cosmogenic radiocarbon events in 774 and 993 CE. *Nature Communications*, *9*(1), 3605. https://doi.org/10.1038/s41467-018-06036-0

Castagnoli, G., & Lal, D. (1980). Solar modulation effects in terrestrial production of carbon-14. *Radiocarbon*, *22*, 133–158. https://doi.org/10.1017/S0033822200009413

Cliver, E. W., Mekhaldi, F., & Muscheler, R. (2020). Solar longitude distribution of high-energy proton flares: Fluences and spectra. *The Astrophysical Journal*, *900*(1), L11. https://doi.org/10.3847/2041-8213/abad44

Delmas, R. J., Beer, J., Synal, H.-A., Muscheler, R., Petit, J.-R., & Pourchet, M. (2004). Bomb-test ^{36}Cl measurements in Vostok snow (Antarctica) and the use of ^{36}Cl as a dating tool for deep ice cores. *Tellus B: Chemical and Physical Meteorology*, *56*(5), 492–498. https://doi.org/10.3402/tellusb.v56i5.16454

Fujita, S, Holmlund, P, Andersson, I, Brown, I, Enomoto, H, Fujii, Y., et al. (2011). Spatial and temporal variability of snow accumulation rate on the East Antarctic ice divide between Dome Fuji and EPICA DML. *The Cryosphere*, *5*, 1057–1081. https://doi.org/10.5194/tc-5-1057-2011

Gleeson, L. J., & Axford, W. I. (1968). Solar modulation of galactic cosmic rays. *The Astrophysical Journal*, *154*, 1011. https://doi.org/10.1086/149822

Grevesse, N., & Sauval, A. J. (1998). Standard solar composition. *Space Science Reviews*, *85*(1/2), 161–174. https://doi.org/10.1023/A:1005161325181

Güttler, D., Adolphi, F., Beer, J., Bleicher, N., Boswijk, G., Christl, M., et al. (2015). Rapid increase in cosmogenic ^{14}C in AD 775 measured in New Zealand kauri trees indicates short-lived increase in ^{14}C production spanning both hemispheres. *Earth and Planetary Science Letters*, *411*, 290–297. https://doi.org/10.1016/j.epsl.2014.11.048

Heikkilä, U. (2007). *Modeling of the atmospheric transport of the cosmogenic radionuclides ^{10}Be and ^{7}Be using the ECHAM5-HAM general circulation model (Doctoral dissertation)*. ETH. https://doi.org/10.3929/ethz-a-005560259

Heikkilä, U., Beer, J., & Feichter, J. (2008). Modeling cosmogenic radionuclides ^{10}Be and ^{7}Be during the maunder minimum using the ECHAM5-HAM general circulation Model. *Atmospheric Chemistry and Physics*, *8*(10), 2797–2809. https://doi.org/10.5194/acp-8-2797-2008

Heikkilä, U., Beer, J., & Feichter, J. (2009). Meridional transport and deposition of atmospheric ^{10}Be. *Atmospheric Chemistry and Physics*, *9*(2), 515–527. https://doi.org/10.5194/acp-9-515-2009

Heikkilä, U., Beer, J., Feichter, J., Alfimov, V., Synal, H.-A., Schotterer, U., et al. (2009). ^{36}Cl bomb peak: Comparison of modeled and measured data. *Atmospheric Chemistry and Physics*, *9*(12), 4145–4156. https://doi.org/10.5194/acp-9-4145-2009

Herbst, K. (2013). Interaction of cosmic rays with the Earth's magnetosphere and atmosphere. (Doctoral thesis), University of Kiel, Germany.

Herbst, K., Heber, B., Beer, J., & Tylka, A. (2015). Modelling the production of cosmogenic radionuclides due to galactic and solar cosmic rays. In *Proceedings of the 34th International cosmic ray conference of science* (Vol. 236). https://doi.org/10.22323/1.236.0537

Herbst, K., Muscheler, R., & Heber, B. (2017). The new local interstellar spectra and their influence on the production rates of the cosmogenic radionuclides ^{10}Be and ^{14}C. *Journal of Geophysical Research: Space Physics*, *122*, 23–34. https://doi.org/10.1002/2016JA023207

Knudsen, M. F., Riisager, P., Donadini, F., Snowball, I., Muscheler, R., Korhonen, K., & Pesonen, L. J. (2008). Variations in the geomagnetic dipole moment during the Holocene and the past 50 kyr. *Earth and Planetary Science Letters*, *272*(1–2), 319–329. https://doi.org/10.1016/j.epsl.2008.04.048

Kovaltsov, G. A., Mishev, A., & Usoskin, I. G. (2012). A new model of cosmogenic production of radiocarbon ^{14}C in the atmosphere. *Earth and Planetary Science Letters*, *337–338*, 114–120. https://doi.org/10.1016/j.epsl.2012.05.036

Kovaltsov, G. A., & Usoskin, I. G. (2010). A new 3D numerical model of cosmogenic nuclide ^{10}Be production in the atmosphere. *Earth and Planetary Science Letters*, *291*(1–4), 182–188. https://doi.org/10.1016/j.epsl.2010.01.011

Laming, J. M., & Feldman, U. (2001). The solar helium abundance in the outer corona determined from observations with SUMER/SOHO. *The Astrophysical Journal*, *546*(1), 552–558. https://doi.org/10.1086/318238

Masarik, J., & Beer, J. (1999). Simulation of particle fluxes and cosmogenic nuclide production in the Earth's atmosphere. *Journal of Geophysical Research: Atmospheres*, *104*(D10), 12099–12111. https://doi.org/10.1029/1998JD200091

Maselli, O. J., Chellman, N. J., Grieman, M., Layman, L., McConnell, J. R., Pasteris, D., et al. (2017). Sea ice and pollution-modulated changes in Greenland ice core methanesulfonate and bromine. *Climate of the Past*, *13*(1), 39–59. https://doi.org/10.5194/cp-13-39-2017

McCracken, K. G., Dreschhoff, G. A. M., Zeller, E. J., Smart, D. F., & Shea, M. A. (2001). Solar cosmic ray events for the period 1561–1950: 1. Identification in polar ice. *Journal of Geophysical Research: Space Physics*, *106*(A10), 21585–21598. https://doi.org/10.1029/2000JA000237

Mekhaldi, F., McConnell, J. R., Adolphi, F., Arienzo, M. M., Chellman, N. J., Maselli, O. J., et al. (2017). No coincident nitrate enhancement events in polar ice cores following the largest known solar storms. *Journal of Geophysical Research: Atmospheres*, *122*(21), 11–900. https://doi.org/10.1002/2017JD027325

Mekhaldi, F., Muscheler, R., Adolphi, F., Aldahan, A., Beer, J., McConnell, J. R., et al. (2015). Multiradionuclide evidence for the solar origin of the cosmic-ray events of AD 774/5 and 993/4. *Nature Communications*, *6*, 8611. https://doi.org/10.1038/ncomms9611

Mewaldt, R. A., Cohen, C. M. S., Labrador, A. W., Leske, R. A., Mason, G. M., Desai, M. I., et al. (2005). Proton, helium, and electron spectra during the large solar particle events of October–November 2003. *Journal of Geophysical Research: Space Physics*, *110*(A9). https://doi.org/10.1029/2005JA011038

Meyer, P., Parker, E. N., & Simpson, J. A. (1956). Solar cosmic rays of February, 1956 and their propagation through interplanetary Space. *Physical Review*, *104*(3), 768–783. https://doi.org/10.1103/PhysRev.104.768

Miyake, F., Masuda, K., & Nakamura, T. (2013). Another rapid event in the carbon-14 content of tree rings. *Nature Communications*, *4*, 1748. https://doi.org/10.1038/ncomms2783

Miyake, F., Nagaya, K., Masuda, K., & Nakamura, T. (2012). A signature of cosmic-ray increase in AD 774–775 from tree rings in Japan. *Nature*, *486*(7402), 240–242. https://doi.org/10.1038/nature11123

Miyake, F., Suzuki, A., Masuda, K., Horiuchi, K., Motoyama, H., Matsuzaki, H., et al. (2015). Cosmic ray event of A.D. 774–775 shown in quasi-annual ^{10}Be data from the Antarctic Dome Fuji ice core. *Geophysical Research Letters*, *42*(1), 84–89. https://doi.org/10.1002/2014GL062218

Muscheler, R., Adolphi, F., Herbst, K., & Nilsson, A. (2016). The revised sunspot record in comparison to cosmogenic radionuclide-based solar activity reconstructions. *Solar Physics*, *291*(9–10), 3025–3043. https://doi.org/10.1007/s11207-016-0969-z

Muscheler, R., Beer, J., Kubik, P. W., & Synal, H.-A. (2005). Geomagnetic field intensity during the last 60,000 years based on ^{10}Be and ^{36}Cl from the Summit ice cores and ^{14}C. *Quaternary Science Reviews*, *24*(16–17), 1849–1860. https://doi.org/10.1016/j.quascirev.2005.01.012

Nilsson, A., Holme, R., Korte, M., Suttie, N., & Hill, M. (2014). Reconstructing Holocene geomagnetic field variation: New methods, models and implications. *Geophysical Journal International*, *198*, 229–248. https://doi.org/10.1093/gji/ggu120

O'Hare, P., Mekhaldi, F., Adolphi, F., Raisbeck, G., Aldahan, A., Anderberg, E., et al. (2019). Multiradionuclide evidence for an extreme solar proton event around 2610 B.P. (~660 BC). *Proceedings of the National Academy of Sciences*, *116*(13), 5961–5966. https://doi.org/10.1073/PNAS.1815725116

Park, J., Southon, J., Fahrni, S., Creasman, P. P., & Mewaldt, R. (2017). Relationship between solar activity and Δ^{14}C peaks in AD 775, AD 994, and 660 BC. *Radiocarbon*, *59*(04), 1147–1156. https://doi.org/10.1017/RDC.2017.59

Pedro, J., Smith, A. M., Duldig, M. L., Klekociuk, A. R., Simon, K. J., Curran, M. A. J., et al. (2009). ^{10}Be concentrations in snow at law dome, antarctica following the 29 October 2003 and 20 January 2005 solar cosmic ray events. In *Advances in Geosciences: Volume 14: Solar Terrestrial (ST)*. (pp. 284–303). https://doi.org/10.1142/9789812836205

Pedro, J., van Ommen, T., Curran, M., Morgan, V., Smith, A., & McMorrow, A. (2006). Evidence for climate modulation of the ^{10}Be solar activity proxy. *Journal of Geophysical Research*, *111*(D21), D21105. https://doi.org/10.1029/2005JD006764

Pivot, S., Baroni, M., Bard, E., & Giraud, X. (2019). A Comparison of ^{36}Cl nuclear bomb inputs deposited in snow from Vostok and Talos Dome, Antarctica, Using the ^{36}Cl/Cl^{-} ratio. *Journal of Geophysical Research: Atmospheres*, *124*(20), 10973–10988. https://doi.org/10.1029/2018JD030200

Poluianov, S. V., Kovaltsov, G. A., Mishev, A. L., & Usoskin, I. G. (2016). Production of cosmogenic isotopes ^{7}Be, ^{10}Be, ^{14}C, ^{22}Na, and ^{36}Cl in the atmosphere: Altitudinal profiles of yield functions. *Journal of Geophysical Research*, *121*(13), 8125–8136. https://doi.org/10.1002/2016JD025034

Raisbeck, G. M., Yiou, F., Fruneau, M., Loiseaux, J. M., Lieuvin, M., & Ravel, J. C. (1981). Cosmogenic ^{10}Be/^{7}Be as a probe of atmospheric transport processes. *Geophysical Research Letters*, *8*(9), 1015–1018. https://doi.org/10.1029/GL008i009p01015

Raukunen, O., Vainio, R., Tylka, A. J., Dietrich, W. F., Jiggens, P., Heynderickx, D., et al. (2018). Two solar proton fluence models based on ground level enhancement observations. *Journal of Space Weather and Space Climate*, *8*, A04. https://doi.org/10.1051/SWSC/2017031

Reames, D. (2004). Solar energetic particle variations. *Advances in Space Research*, *34*(2), 381–390. https://doi.org/10.1016/J.ASR.2003.02.046

Shea, M. A., & Smart, D. F. (2012). Space weather and the ground-level solar proton events of the 23rd solar cycle. *Space Science Reviews*, *171*(1–4), 161–188. https://doi.org/10.1007/s11214-012-9923-z

Sigl, M., Winstrup, M., McConnell, J. R., Welten, K. C., Plunkett, G., Ludlow, F., et al. (2015). Timing and climate forcing of volcanic eruptions for the past 2,500 years. *Nature*, *523*(7562), 543–549. https://doi.org/10.1038/nature14565

Simpson, J. A. (1960). The production of tritons and ^{14}C in the terrestrial atmosphere by solar protons. *Journal of Geophysical Research*, *65*(5), 1615–1616. https://doi.org/10.1029/jz065i005p01615

Simpson, J. A. (2000). The cosmic ray nucleonic component: The invention and scientific uses of the neutron monitor. *Space Science Reviews*, *93*(11), 11–32. https://doi.org/10.1023/a:1026567706183

Škerlak, B., Sprenger, M., & Wernli, H. (2014). A global climatology of stratosphere–troposphere exchange using the ERA-Interim data set from 1979 to 2011. *Atmospheric Chemistry and Physics*, *14*(2), 913–937. https://doi.org/10.5194/acp-14-913-2014

Steinhilber, F., Abreu, J. A., Beer, J., Brunner, I., Christl, M., Fischer, H., et al. (2012). 9400 Years of cosmic radiation and solar activity from ice cores and tree rings. *Proceedings of the National Academy of Sciences*, *109*(16), 5967–5971. https://doi.org/10.1073/pnas.1118965109

Stohl, A., Bonasoni, P., Cristofanelli, P., Collins, W., Feichter, J., Frank, A., et al. (2003). Stratosphere-troposphere exchange: A review, and what we have learned from STACCATO. *Journal of Geophysical Research Atmospheres*, *108*(12). https://doi.org/10.1029/2002jd002490

Stuiver, M., & Polach, H. A. (1977). Discussion Reporting of ^{14}C Data. *Radiocarbon*, *19*(03), 355–363. https://doi.org/10.1017/S0033822200003672

Sukhodolov, T., Usoskin, I., Rozanov, E., Asvestari, E., Ball, W. T., Curran, M. A. J., et al. (2017). Atmospheric impacts of the strongest known solar particle storm of 775 AD. *Scientific Reports*, *7*(1), 45257. https://doi.org/10.1038/srep45257

Synal, H.-A., Beer, J., Bonani, G., Suter, M., & Wölfli, W. (1990). Atmospheric transport of bomb-produced ^{36}Cl. *Nuclear Instruments and Methods in Physics Research Section B: Beam Interactions with Materials and Atoms*, *52*(3–4), 483–488. https://doi.org/10.1016/0168-583X(90)90462-4

Usoskin, I. G., Gil, A., Kovaltsov, G. A., Mishev, A. L., & Mikhailov, V. V. (2017). Heliospheric modulation of cosmic rays during the neutron monitor era: Calibration using PAMELA data for 2006−−2010. *Journal of Geophysical Research: Space Physics*, *122*(4), 3875–3887. https://doi.org/10.1002/2016JA023819

Usoskin, I. G., Koldobskiy, S. A., Kovaltsov, G. A., Rozanov, E. V., Sukhodolov, T. V., Mishev, A. L., & Mironova, I. A. (2020). Revisited reference solar proton event of 23 February 1956: Assessment of the cosmogenic-isotope method sensitivity to extreme solar events. *Journal of Geophysical Research: Space Physics*, *125*(6). https://doi.org/10.1029/2020JA027921

Usoskin, I. G., & Kovaltsov, G. A. (2012). Occurrence of extreme solar particle events: Assessment from historical proxy data. The *Astrophysical Journal*, *757*(1), 92. https://doi.org/10.1088/0004-637X/757/1/92

Usoskin, I. G., Kromer, B., Ludlow, F., Beer, J., Friedrich, M., Kovaltsova, G., et al. (2013). The AD775 cosmic event revisited: The Sun is to blame. *Astronomy & Astrophysics*, *775*, 1–8. https://doi.org/10.1051/0004-6361/201321080

Usoskin, I. G., Solanki, S. K., Kovaltsov, G. A., Beer, J., & Kromer, B. (2006). Solar proton events in cosmogenic isotope data. *Geophysical Research Letters*, *33*(8), L08107. https://doi.org/10.1029/2006GL026059

Uusitalo, J., Arppe, L., Hackman, T., Helama, S., Kovaltsov, G., Mielikäinen, K., et al. (2018). Solar superstorm of AD 774 recorded subannually by Arctic tree rings. *Nature Communications*, *9*(1), 3495. https://doi.org/10.1038/s41467-018-05883-1

Vonmoos, M., Beer, J., & Muscheler, R. (2006). Large variations in Holocene solar activity: Constraints from ^{10}Be in the Greenland Ice Core Project ice core. *Journal of Geophysical Research*, *111*(A10), A10105. https://doi.org/10.1029/2005JA011500

von Steiger, R., Schwadron, N. A., Fisk, L. A., Geiss, J., Gloeckler, G., Hefti, S., et al. (2000). Composition of quasi-stationary solar wind flows from Ulysses/Solar Wind Ion Composition Spectrometer. *Journal of Geophysical Research: Space Physics*, *105*(A12), 27217–27238. https://doi.org/10.1029/1999JA000358

Wagner, G., Masarik, J., Beer, J., Baumgartner, S., Imboden, D., Kubik, P. W., et al. (2000). Reconstruction of the geomagnetic field between 20 and 60 kyr BP from cosmogenic radionuclides in the GRIP ice core. *Nuclear Instruments and Methods in Physics Research Section B: Beam Interactions with Materials and Atoms*, *172*(1), 597–604. https://doi.org/10.1016/S0168-583X(00)00285-8

Webber, W. R., Higbie, P. R., & McCracken, K. G. (2007). Production of the cosmogenic isotopes ^{3}H, ^{7}Be, ^{10}Be, and ^{36}Cl in the Earth's atmosphere by solar and galactic cosmic rays. *Journal of Geophysical Research*, *112*(A10), A10106. https://doi.org/10.1029/2007JA012499

Zheng, M., Adolphi, F., Sjolte, J., Aldahan, A., Possnert, G., Wu, M., et al. (2020). Solar and climate signals revealed by seasonal ^{10}Be data from the NEEM ice core project for the neutron monitor period. *Earth and Planetary Science Letters*, *541*, 116273. https://doi.org/10.1016/j.epsl.2020.116273